A Universal Single Stage Current-fed Bidirectional Converter with both AC and DC Input Power Source Compatibility

Manish Kumar, Sumit Pramanick and Bijaya Ketan Panigrahi
Department of Electrical Engineering, Indian Institute of Technology, Delhi
Email: manish.kumar@ee.iitd.ac.in

Acknowledgments

Keywords

Abstract

This article demonstrates a universal, single power conversion stage (1-S) current-fed bidirectional converter based on-board electric vehicle (EV) charger (OBC). The converter can be connected to either residential ac utility gird or solar photovoltaic (PV) array. Additionally, when connected to ac grid, the converter maintains unity power factor (UPF) and when connected to PV array, the power is extracted at the maximum power point (MPP). A laboratory prototype of 1.5 kW is developed to validate the theoretical analysis and can be connected to 230 V, 50 Hz ac mains voltage or 100-300 V PV array. The battery voltage range is of 300-400 V.

1 Introduction

Advancements in battery technology, charging infrastructures, and efficient drive trains, electric vehicles (EVs) have grown in popularity and customer acceptability. As shown in Fig. 1a, EVs power systems generally comprises of drivetrain, on-board charger (OBC), auxiliary power module (APM) and motor drive inverter [1]. OBC is an integral part of EV as it allows the customer to charge their vehicle overnight using a residential ac utility grid.

General design criteria for OBCs is to meet power quality requirements on the grid side, as defined by IEEE 519 standards [2]. In addition, galvanic isolation between the power source and the vehicle battery is required for safety requirements as defined by Underwriters Laboratories (UL) 2202 standards [3]. Furthermore, owing to space constraints in EVs, OBCs should have high volumetric and electrical efficiency. These design requirements are met by OBCs with two power conversion stages (2-S). The first stage is a power factor correction (PFC), while the second stage is an isolated dc-dc converter [4,5]. A 2-S based OBCs have increased component counts, resulting in higher losses.

To overcome the drawbacks of 2-S based OBCs, several single power conversion stage (1-S) OBCs have been explored. In [6,7], a 1-S bridgeless ac–dc converter with power factor correction for EV charging has been reported. However, these converters lack galvanic isolation, as required by safety standards. [8] showed a 1-S half-bridge matrix convert with combined frequency and phase shift modulation and [9] proposed an optimal zero voltage switching (ZVS) modulation for DAB-based converter, but requires an additional line frequency synchronous rectifier on the grid side. Additionally, the above mentioned
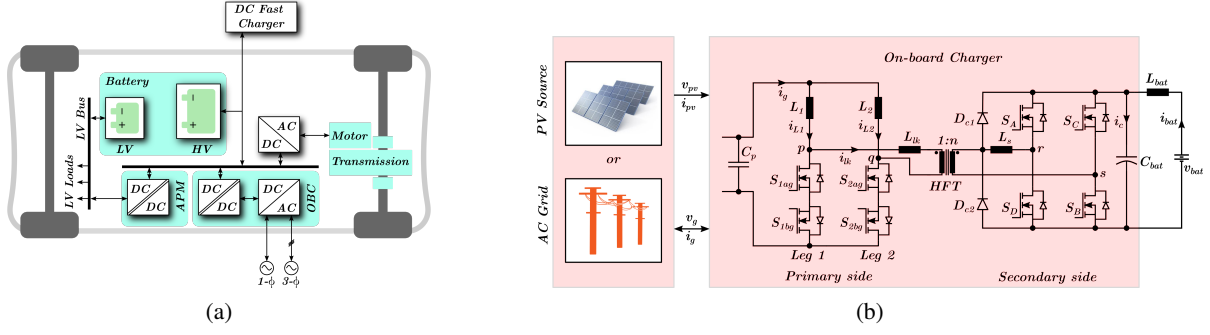
Fig. 1: (a) EV power system architecture. (b) L-L type current-fed half bridge bidirectional converter.

converters can only be connected to ac residential grid and therefore are classified as isolated ac-dc power converters. The charger developed in [10, 11] connects only to solar photovoltaic (PV) array to charge the battery.

This paper demonstrates a 1-S L-L type current-fed half-bridge (CFHB) bidirectional converter with both ac and dc input power source compatibility. The CFHB is a good alternative to voltage-fed converters due to reduced input current ripple, efficient performance over a wide input range, and easier input current controllability [12]. Furthermore, the converter can be connected to a residential ac utility grid and draw power at unity power factor (UPF). The converter can also be connected to a PV array in the absence of ac grid and extract power at the maximum power point (MPP).

The paper is organized as follows: section 2 provides the detailed description of the converter along with the operation. Experimental results are presented and discussed in section 3. Lastly, conclusions are given in section 4.

2 Converter Description and Operation

2.1 Converter description

Fig. 1b depicts the schematic of a 1-S galvanically isolated current-fed half bridge bidirectional converter. On the primary side, it consists of a current-fed half bridge converter with bidirectional switches, and on the secondary side, it consists of a voltage-fed full bridge converter connected via a high frequency transformer (HFT). The two boost inductors are L_1 and L_2. The HFT's leakage inductance is L_{lk}. To obtain the necessary total series inductance $L_t = L_{lk} + L_s/n^2$, an external series inductor L_s is added on the secondary side. The primary and secondary side filter capacitors are denoted by C_p and C_{bat} respectively. D_{c1} and D_{c2} are the diode clamps that prevents parasitic ringing across the primary side switches.

2.2 Converter Operation

The 1-S converter can be connected to either a residential ac utility grid or solar PV array. The switching scheme when connected to ac utility grid is based on improved discontinuous current phase shift modulation (IDCPSM) and is described as follows. Primary side switches S_{1ag} and S_{2ag} are switched at a duty ratio of $d_1^{(k)} > 0.5$ in the positive half cycle of grid voltage and is continuously on in the negative half cycle. Similarly, S_{1bg} and S_{2bg} are switched at a duty ratio of $d_1^{(k)}$ in the negative half cycle of grid voltage and is continuously on in the positive half cycle. Secondary side switches S_A and S_D are switched at a fixed duty ratio of 0.5. S_B and S_C are switched at a variable duty ratio of $d_2^{(k)}$. The switching scheme when connected to solar PV array remains same and depending on the connection polarity, the corresponding primary side switching combination is applied. Fig. 2 shows the operation waveform of the converter in a grid cycle along with the switching interval waveform shown in the zoomed section.

Following assumption are made for simplifying the analysis of the converter.

- When connected to a domestic ac grid, the converter operates at UPF.
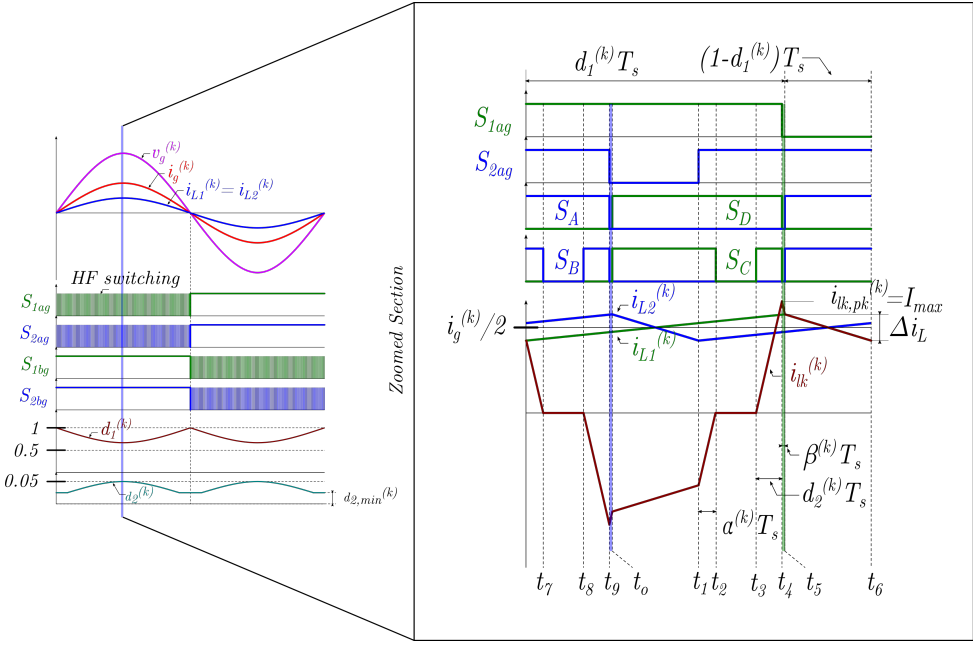
Fig. 2: Operational waveform of the converter in a grid cycle.

- In a switching interval k, the input grid voltage v_g and grid current i_g are assumed to be constant and is given by (1) and (2) respectively.

- For high switching operation, the effect of parasitic capacitance and device output capacitance are ignored.

$$v_g^{(k)}(kT_s) = V_m sin(\omega kT_s) \tag{1}$$

$$i_g^{(k)}(kT_s) = \frac{2P_o}{V_m} sin(\omega kT_s) \tag{2}$$

Primary side duty cycle is given by

$$d_1^{(k)} = \frac{V_{bat} - n|v_g^{(k)}(kT_s)|}{V_{bat}} \tag{3}$$

Secondary side duty cycle is given by

$$d_2^{(k)} = \frac{nL_t|i_{lk,pk}^{(k)}|}{V_{bat}T_s} \tag{4}$$

where, $\omega = 2\pi/t_g$, t_g is the time period of a grid cycle, T_s is the time period of a switching cycle.

2.3 AC utility grid operation

The OBC when connected to ac utility grid, a dual control variable approach proposed in [13] has been adopted. In this control structure, the primary side duty $d_1^{(k)}$ is modulated to maintain UPF. In addition, to minimize the peak circulating current flowing through the HFT, secondary side duty $d_2^{(k)}$ is modulated across the grid cycle of ac mains voltage. The nature of primary and secondary side duty in a grid cycle is depicted in Fig. 2. Furthermore, throughout the operation, ZCS turn-off is achieved for primary side switches and ZVS turn-on is achieved for secondary side switches. This results in very low conduction and switching losses.
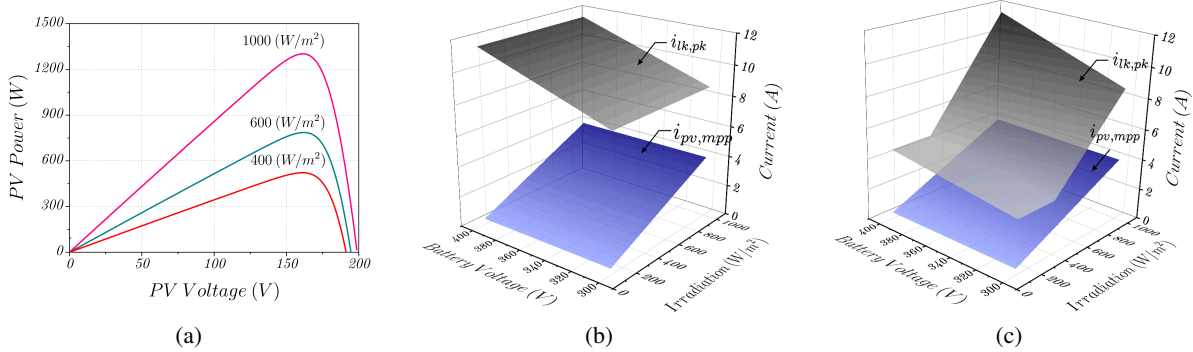
Fig. 3: (a) PV curve for different irradiation conditions, (b) variation of transformer winding peak current $i_{lk,pk}$ and MPP PV array current $i_{pv,mpp}$ for different battery voltage and irradiation at fixed secondary side duty and (c) varying secondary side duty

2.4 PV array operation

The OBC when connected to PV array, a similar dual control variable approach is developed. This control structure allows for MPPT by modulating the primary side duty $d_1^{(k)}$ using adaptive incremental conductance algorithm [14]. The secondary side duty $d_2^{(k)}$ can be kept fixed to 0.05 for active current commutation as proposed in [15]. However, the MPP of the PV array reduces under low irradiation conditions as depicted by the PV curve in Fig. 3a. Therefore, from (4) it can be concluded that for a fixed battery voltage, the peak value of transformer winding current would remain fixed irrespective of the irradiation condition. This means that for low irradiation conditions, the circulating current through the transformer winding would be substantially high as depicted in Fig. 3b, thereby contributing to higher losses. In order to minimize the circulating at low irradiation conditions, the secondary side duty $d_2^{(k)}$ is varied in this control structure. This can be seen observed in Fig. 3c that for varying irradiation, the peak current through the transformer winding is closely following the MPP PV array current, thereby substantially reducing the losses in the converter.

2.4 Current expressions

For detailed loss analysis, the section provides this current expressions flowing through the various components of the converter when connected to ac grid. Same expressions are used when connected to PV array by assuming $t_g = T_s$

- Primary side HFT RMS current

$$I_{lk,RMS} = \sqrt{\frac{T_s}{t_g} \sum_{k=1}^{t_g/T_s} \frac{(i_g^{(k)})^2}{2} \left(1 - d_1^{(k)} + \frac{4d_2^{(k)}}{3} + \frac{\alpha^{(k)}}{3} + \frac{7\beta^{(k)}}{3} \right)} \tag{5}$$

- Primary side switch RMS current

$$I_{S_{pri,RMS}} = \sqrt{\frac{T_s}{t_g} \sum_{k=1}^{t_g/T_s} \left(\frac{i_g^{(k)}}{2} \right)^2 \left(\frac{11}{3} - \frac{10d_1^{(k)}}{3} + 4d_2^{(k)} + \frac{7\alpha^{(k)}}{3} + \frac{17\beta^{(k)}}{3} \right)} \tag{6}$$

- Primary side switch body diode average current

$$I_{D_{pri,avg}} = \frac{T_s}{t_g} \sum_{k=1}^{t_g/T_s} \frac{i_g^{(k)}}{2} \frac{\beta^{(k)}}{2} \tag{7}$$
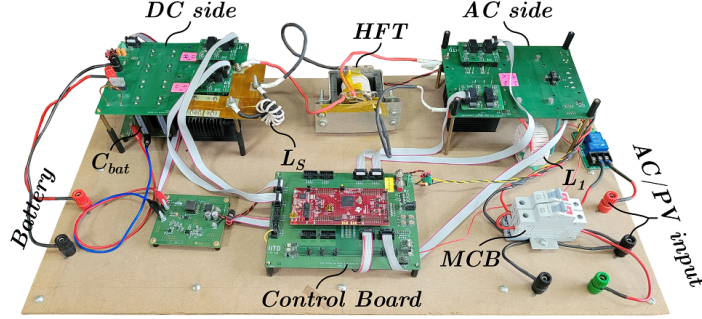
Fig. 4: Laboratory prototype of L-L type current fed half bridge bidirectional converter.

Table I: Experimental Setup Parameters

Converter Parameters		PV Panel Parameters	
Descriptions	**Specifications**	**Descriptions**	**Specifications**
Power Rating (P_o)	1.5 kW	Maximum Power ($P_{pv,MPP}$)	0.325 kW
Input Grid Voltage (V_g)	230 V	MPP Voltage ($v_{pv,MPP}$)	40 V
Battery Voltage (V_{bat})	300...400 V	Open Circuit Voltage ($v_{pv,OC}$)	50 V
Transformer Turns ratio (n) and Leak Inductance (L_{lk})	0.37 and 6.5 μH	No. of Panel in series	4
Boost Inductor (L_1) and (L_2)	1.5 mH	Model	Kyocera Solar KD325GX
Primary side filter Capacitor (C_p)	4.7 μF		
Secondary side filter Capacitor (C_{bat})	100 μF		
Switching Frequency (f_{sw})	100 kHz		
Primary side Mosfets (S_{xyg})	C2M0080170P		
Secondary side Mosfets (S_p)	UF3C065030K4S		

- Secondary side switch RMS current

$$I_{S_{sec,RMS}} = \sqrt{\frac{T_s}{t_g} \sum_{k=1}^{t_g/T_s} \left(\frac{i_g^{(k)}}{2n}\right)^2 \left(1 - d_1^{(k)} + \frac{4d_2^{(k)}}{3} + \frac{\alpha^{(k)}}{3} + \frac{7\beta^{(k)}}{3}\right)} \qquad (8)$$

3 Experimental Results and Discussion

To evaluate the converter's performance with both ac and dc input power sources, a 1.5-kW laboratory prototype is developed as shown in Fig. 4. The ac input source is 230V, 50Hz, and the dc input is via a PV emulator. The parameters of the experimental setup are listed in Table I. A TI TMS320F28397D launchpad is used to implement the control scheme, and a Xilinx XC6SLX4-based FPGA board is used to generate the gate pulse combinational logic.

3.1 Experimental waveform

The measured ac grid voltage v_g, grid current i_g, battery current i_{bat} and primary side HFT winding current i_{lk} for few grid cycle is shown in Fig. 5a. It is evident from the figure that converter is operating at 0.999 power factor and $P_o = 1.5\,kW$. The primary side HFT winding current has a sinusoidal envelope

with a frequency that is twice that of the ac mains voltage. The measured primary side v_{pq} and secondary side v_{rs} HFT voltage and primary side HFT winding current i_{lk} for a few switching interval is shown in Fig. 5b.


(a)

(b)
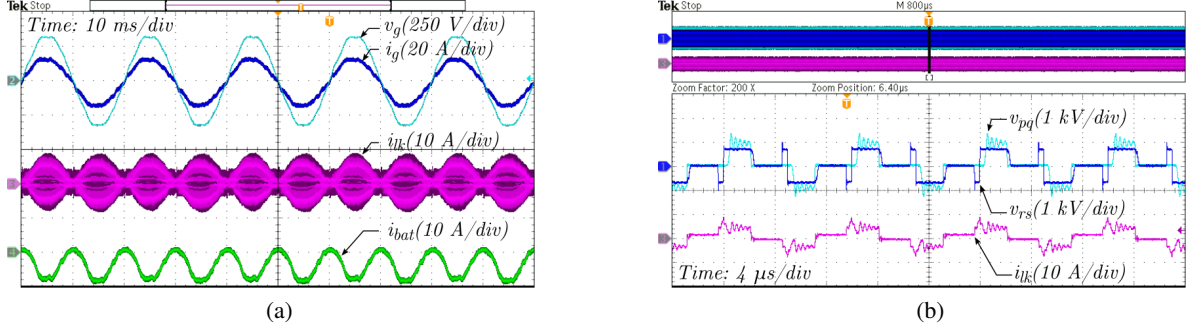
Fig. 5: (a) Measured grid voltage v_g, grid current i_g, battery current i_{bat} and primary side HFT winding current i_{lk} ($P_o = 1.5\,kW$, $v_g = 230\,V_{rms}$ and $V_{bat} = 345\,V$), (b) measured primary side v_{pq} and secondary side v_{rs} HFT voltage and primary side HFT winding current i_{lk} in a few switching interval.

(a)

(b)
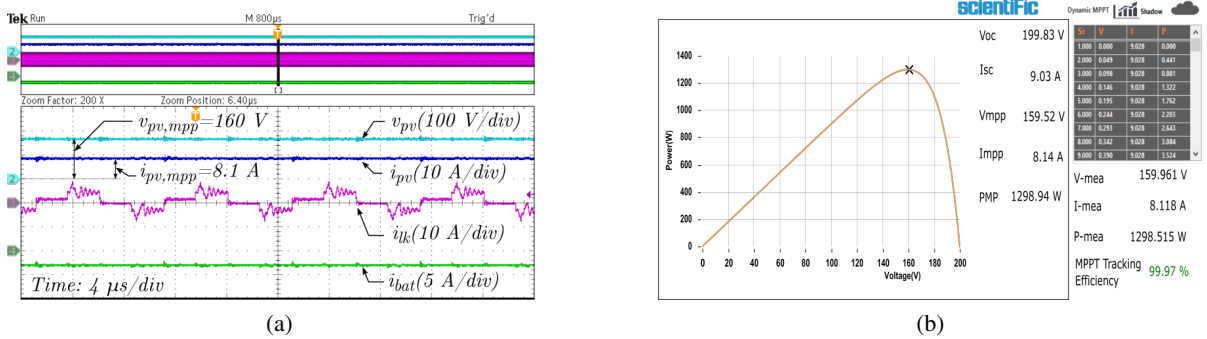
Fig. 6: (a) Measured PV voltage v_{pv}, PV current i_{pv}, battery current i_{bat} and primary side HFT winding current i_{lk} ($P_{pv,mpp} = 1.3\,kW$ and $V_{bat} = 345\,V$), (b) PV emulator software showing MPP tracking efficiency.

(a)

(b)
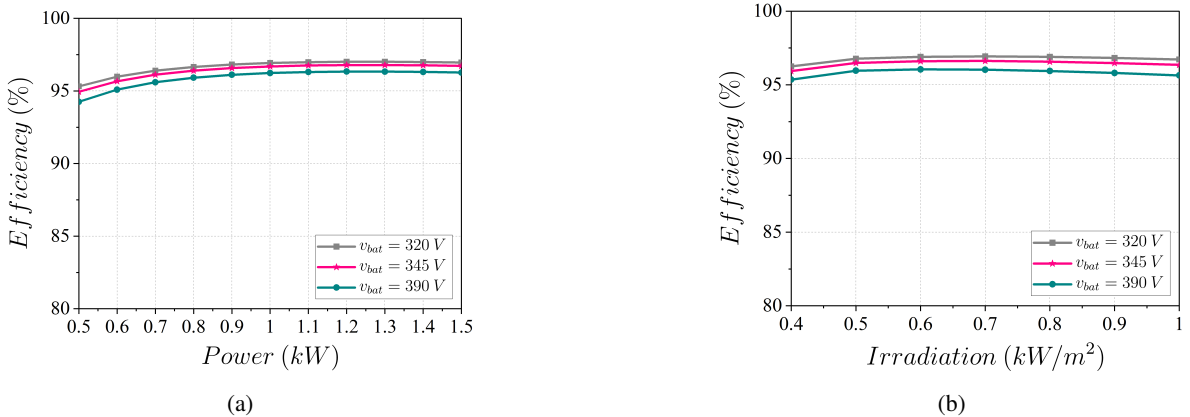
Fig. 7: Efficiency curve for different battery voltage V_{bat} (a) grid connected varying loading conditions (b) PV connected varying irradiation conditions.

It can be clearly observed from Fig. 6a showing the measured PV voltage v_{pv}, PV current i_{pv}, battery current i_{bat} and primary side HFT winding current i_{lk}, that the converter is extracting power from the PV

array at MPP i.e. $P_{pv,mpp} = 1.3\,kW$. This can be also seen in Fig. 6b showing the MPP tracking efficiency of 99.97% from PV emulator software.

3.1 Efficiency

Fig. 7a and 7b shows the theoretical efficiency cure for different battery voltage V_{bat} when connected to ac grid and PV array respectively. A peak efficiency of 97.01% is observed when operated in grid connected mode and peak efficiency of 96.92% and almost a flat efficiency profile across irradiation conditions is seen when connected to PV array.

4   Conclusion

A universal, 1-S current-fed bidirectional converter as an OBC has been demonstrated in this article. The converter is compatible with both ac and dc input power source i.e. it can be connected to either residential ac utility gird or PV array. The converter draws power at UPF from the ac grid and the power is extracted at the MPP when connected to PV array. The IDCPSM switching scheme has been modified to minimize circulating current across varying irradiation conditions. Peak efficiency of 97.01% when connected to ac grid and 96.92% when connected to PV array is achieved.

References

[1] A. Khaligh and M. D'Antonio, "Global Trends in High-Power On-Board Chargers for Electric Vehicles," IEEE Trans. Veh. Technol., vol. 68, no. 4, pp. 3306–3324, Apr. 2019.

[2] "IEEE Recommended Practice and Requirements for Harmonic Control in Electric Power Sys- tems," IEEE Std 519-2014 Revis. IEEE Std 519-1992, pp. 1–29, Jun. 2014.

[3] "UL-2202StandardforElectricVehicle(EV)ChargingSystemEquipment—StandardsCatalog," https://standardscatalog.ul.com/standards/en/standard 2202 2.

[4] J. Lu, K. Bai, A. R. Taylor, G. Liu, A. Brown, P. M. Johnson, and M. McAmmond, "A Modular-Designed Three-Phase High-Efficiency High-Power-Density EV Battery Charger Using Dual/Triple-Phase-Shift Control," IEEE Trans. Power Electron., vol. 33, no. 9, pp. 8091–8100, Sep. 2018.

[5] B.-K. Lee, J.-P. Kim, S.-G. Kim, and J.-Y. Lee, "An Isolated/Bidirectional PWM Resonant Con- verter for V2G(H) EV On-Board Charger," IEEE Trans. Veh. Technol., vol. 66, no. 9, pp. 7741– 7750, Sep. 2017.

[6] B. R. Ananthapadmanabha, R. Maurya, and S. R. Arya, "Improved Power Quality Switched In- ductor Cuk Converter for Battery Charging Applications," IEEE Trans. Power Electron., vol. 33, no. 11, pp. 9412–9423, Nov. 2018.

[7] J. Gupta, R. Kushwaha, and B. Singh, "Improved Power Quality Transformerless Single-Stage Bridgeless Converter Based Charger for Light Electric Vehicles," IEEE Trans. Power Electron., vol. 36, no. 7, pp. 7716–7724, Jul. 2021.

[8] F. Jauch and J. Biela, "Combined Phase-Shift and Frequency Modulation of a Dual-Active-Bridge AC–DC Converter With PFC," IEEE Trans. Power Electron., vol. 31, no. 12, pp. 8387–8397, Dec. 2016.

[9] J. Everts, F. Krismer, J. V. den Keybus, J. Driesen, and J. W. Kolar, "Optimal ZVS Modulation of Single-Phase Single-Stage Bidirectional DAB AC–DC Converters," IEEE Trans. Power Electron., vol. 29, no. 8, pp. 3954–3970, Aug. 2014.

[10] J. Traube, F. Lu, D. Maksimovic, J. Mossoba, M. Kromer, P. Faill, S. Katz, B. Borowy, S. Nichols, and L. Casey, "Mitigation of Solar Irradiance Intermittency in Photovoltaic Power Systems With Integrated Electric-Vehicle Charging Functionality," IEEE Trans. Power Electron., vol. 28, no. 6, pp. 3058–3067, Jun. 2013.

[11] S.Biswas,L.Huang,V.Vaidya,K.Ravichandran,N.Mohan,andS.V.Dhople,"UniversalCurrent- Mode Control Schemes to Charge Li-Ion Batteries Under DC/PV Source," IEEE Trans. Circuits Syst. Regul. Pap., vol. 63, no. 9, pp. 1531–1542, Sep. 2016.

[12] K. Gnanasambandam, A. K. Rathore, A. Edpuganti, D. Srinivasan, and J. Rodriguez, "Current-Fed Multi-level Converters: An Overview of Circuit Topologies, Modulation Techniques, and Applica- tions," IEEE Trans. Power Electron., vol. 32, no. 5, pp. 3382–3401, May 2017.

[13] M. Kumar, S. Pramanick, and B. K. Panigrahi, "Reduction in Circulating Current With Improved Secondary Side Modulation in Isolated Current-Fed Half Bridge AC–DC Converter," IEEE Trans. Power Electron., vol. 37, no. 5, pp. 5625–5636, May 2022.

[14] E. Kim, M. Warner, and I. Bhattacharya, "Adaptive Step Size Incremental Conductance Based Maximum Power Point Tracking (MPPT)," in 2020 47th IEEE Photovoltaic Specialists Conference (PVSC), Jun. 2020, pp. 2335–2339.

[15] U. R. Prasanna, A. K. Rathore, and S. K. Mazumder, "Novel Zero-Current-Switching Current-Fed Half-Bridge Isolated DC/DC Converter for Fuel-Cell-Based Applications," IEEE Trans. Ind. Appl., vol. 49, no. 4, pp. 1658–1668, Jul. 2013.